Aerodynamic wind tunnel testing of a generic Hypersonic Glide Vehicle

T. Gawehn, J. Zhai, P. Gruhn, A. Gülhan 1

Abstract

Static and dynamic aerodynamic wind tunnel tests are performed on the Generic Hypersonic Glide Vehicle 1 (GHGV-1) designed by DLR. Two facilities at DLR Cologne are used to cover a test Mach range from Ma=8.8 down to Ma=2.0. The performance of the vehicle is investigated with respect to different aspects like trim ability, efficiency of the control surfaces or dynamic stability. Experimental data are compared to the results of a numerical simulation. Additionally, flow structures are visualised by means of Schlieren optic and oil flow visualisation. The aerodynamic performance is found promising so that in a further step the investigation will be extended to the determination of dynamic roll derivatives.

Keywords: Hypersonic aerodynamics, Glide vehicle, Wind tunnel testing, Free oscillation

Nomenclature

Latin		Greek	
С	Coefficient	α	Angle of attack
C_{mlpha}	Aerodynamic stiffness	β	Sideslip angle
$C_{mq} + C_{m\dot{\alpha}}$	Aerodynamic damping	δ	Damping decrement
D	Drag	κ	Ratio of specific heats
Н	Altitude	ho	Density
I	Moment of inertia	θ	Deflection angle
L	Length / Lift	ϕ	Roll angle
Ma	Mach number	ω	Angular frequency
$M_{ heta}$	Aerodynamic stiffness.		
$M_{\dot{ heta}}$	Aerodynamic damping	Subscripts	
Re	Reynolds number	defl	Deflection
S	Surface	F	Force related
С	Mechanical Stiffness	M	Moment related
k	Mechanical damping	pB	Base pressure related
m	Mass	Ref	Reference
p	Pressure	trim	Trim condition
q	Dynamic pressure	x, y, z	Related to axis direction
t	Time	0	Stagnation/aligned condition
u	Velocity	∞	Freestream condition

1. Introduction

The German Aerospace Center (DLR) focusses its research into missile technologies on the development of technologies suited to improve the performance of future missile systems, and on the development of tools and methods to analyse and assess the performance and capabilities of missile systems. Thereby, a strong focus of its work is on hypersonic missiles. Since the work is dedicated more towards general analysis than towards existing systems, and information on such systems is anyway usually either classified or from questionable open source references, the analysis is usually based on generic

HiSST-2025-0013
Aerodynamic wind tunnel testing of a generic Hypersonic Glide Vehicle

¹ German Aerospace Center (DLR), Institute of Aerodynamics and Flow Technology, Supersonic and Hypersonic Technologies Department, Linder Höhe, 51147 Köln, Germany, Thomas.gawehn@dlr.de

reference vehicles, which are representative of realistic threats. The Generic Hypersonic Glide Vehicle 1 (GHGV-1) was designed for this purpose by DLR [1]. Further information about and results of the study on the GHGV-1 can be found in [2, 3].

1.1. GENERIC HYPERSONIC GLIDE VEHICLE 1 (GHGV-1)

The GHGV-1 is a generic design of a tactical Hypersonic Glide Vehicle with a design Mach number of Mach 10 [1]. It is designed as a Boost-Glide Vehicle, i.e. it is launched by a booster rocket on a depressed ballistic trajectory, and then released at high altitudes (near the von Karman line; $H=100\ km$). Until separation, the cruise stage sits under a fairing, for environmental protection and aerodynamic considerations. After separation from the booster stage, the GHGV-1 re-enters the atmosphere and glides towards its target. To improve its gliding capabilities, the cruise stage is designed as a conical wave rider. Two integrated flaps on the bottom surface and two fins on the upper side are used for control and for stabilizing the vehicle aerodynamically during atmospheric flight. At higher altitudes, small thrusters located at the rear of the vehicle are used for attitude control. A render image of GHGV-1 is shown in Fig. 1.

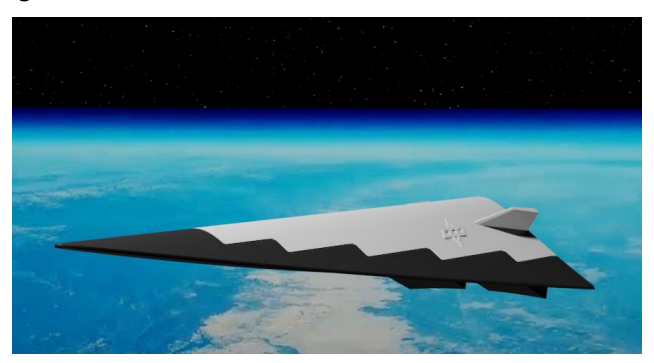


Fig. 1 Render image of Generic Hypersonic Glide Vehicle GHGV-1

1.2. APPROACH

The approach of the GHGV-1 investigation is visualised in Fig. 2, left. The investigation starts with an initial design of the aeroshape of the GHGV-1. Then, numerical simulations are performed and an aerodynamic database is built. Based on this database, a flight dynamic analysis is performed and mission scenarios are developed. The flight path of one such scenario is shown in Fig. 2 (right hand side) as Mach number and altitude over flight time. Based on the results, a back-loop to a design change might be necessary at different points.

As the first step in the following *Specification Phase*, wind tunnel models are designed and built to perform at first static aerodynamic tests and then dynamic wind tunnel tests. The results of these tests are implemented into the aerodynamic database together with further numerical simulation data to reperform the flight dynamic analysis and end up with an improved mission scenario. Also, in this phase, a back-loop to a design change might be caused.

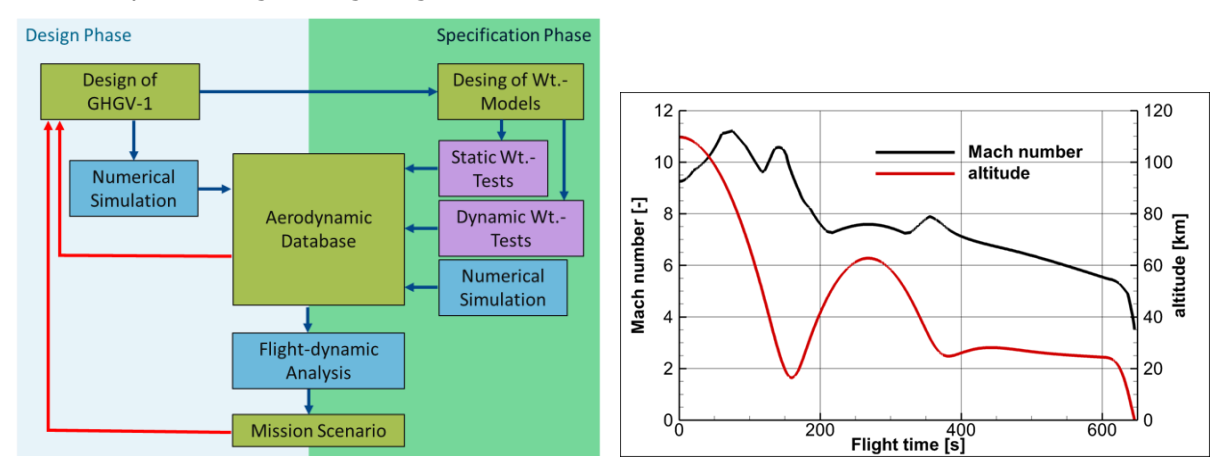


Fig. 2. Approach of investigation (left), flight trajectory of initial mission scenario (right)

1.3. CONTENT OF THIS PAPER

The investigation of the GHGV-1 is ongoing. This publication presents an extract of the experimental results currently available: static aerodynamic and flow visualisation data of the covered Mach range from Ma=8.8 down to Ma=2 and dynamic derivatives of the pitch motion in the hypersonic regime. Dynamic tests regarding the roll behaviour are currently under preparation. In the frame of this publication, only an extract of the results can be presented.

2. EXPERIMENTAL SETUP

2.1. HYPERSONIC WIND TUNNEL COLOGNE (H2K)

The H2K facility of DLR (schematic in Fig. 3, left) is a blow-down wind tunnel. In this setup, pressurized air from a reservoir with up to 55 bar, is introduced into the tunnel. To prevent condensation and facilitate operation at various stagnation temperatures, electrical heaters with a heating capacity of up to $5\,MW$ are used to heat the air, that is first blown into the atmosphere during the heating process until the desired stationary stagnation conditions are achieved. Then, a 3/2 way valve is activated to allow the air to flow through a contoured axisymmetric nozzle, which has an exit diameter of $600\,mm$, before entering a free-jet test section equipped with large quartz glass windows on opposing sides to enable direct optical access to the flow. Subsequently, the exhaust flow is directed into a vacuum sphere. Thanks to the independent control of pressure and temperature, adjustments to the Reynolds number and dynamic pressure can be made separately [4].

With different contoured axisymmetric nozzles, the H2K covers a nominal test range from Ma = 5.3 up to 11.2. Depending on the Mach number a unit Reynolds number of more than $Re = 20 \, Mio/m$ can be achieved. The performance map of the wind tunnel is visualised in Fig. 3 (right).

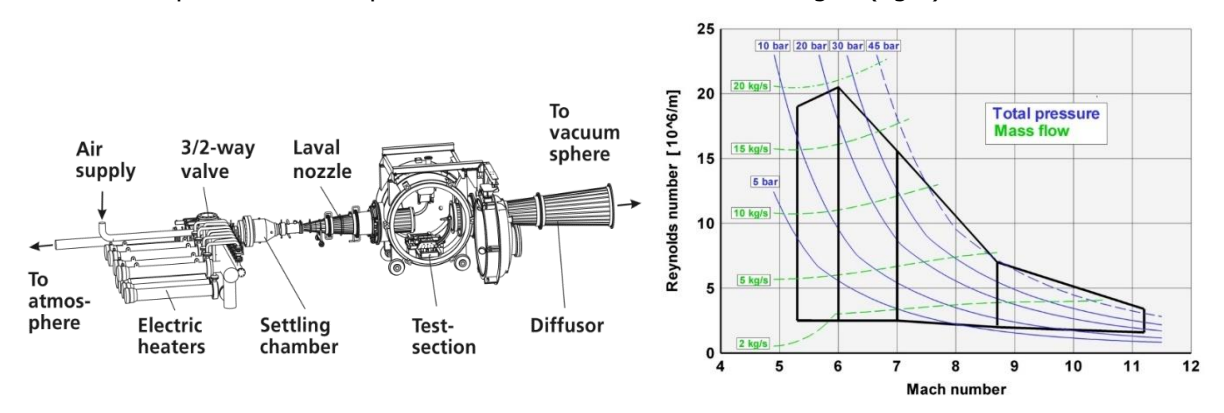


Fig. 3. Schematic (left) and performance map (right) of wind tunnel H2K

2.2. TRISONIC WIND TUNNEL COLOGNE (TMK)

The TMK facility of DLR is a trisonic blow down wind tunnel with a rectangular test section of $0.6\ m\ x\ 0.6\ m$. It is equipped with large quartz glass windows on opposing sides, providing direct optical access to the test section. As sketched in Fig. 4 (left), air from a $55\ bar$ pressure reservoir passes a storage heater and a settling chamber and is then accelerated in an adaptable de Laval nozzle. In the test section, the flow conditions are nearly constant. The flow is decelerated downstream in the diffuser system. Depending on Mach and Reynolds conditions, a maximum testing time of up to 60 seconds is achieved [5].

The performance map of the facility is given in Fig. 4 (right). The standard Mach number range in the supersonic operation mode is 1.25 < Ma < 4.5. The wind tunnel is operated at a dynamic pressure of $q_{\infty} \approx 1 \ bar$ in this range. The Mach number is controlled via the adaptable de Laval nozzle. The diffuser is usually fully open. Tests with reduced dynamic pressure or Mach numbers up to Ma = 5.7 can be realized by ejecting additional air mass flow downstream the subsonic diffuser and, if necessary, by additionally heating the flow in the storage heater.

For Mach numbers of 0.5 < Ma < 1.2, an additional transonic test section with perforated walls of

variable aperture is installed downstream the supersonic test section. In this case, the wind tunnel is operated at a static pressure of $p_{\infty} \approx 1~bar$ and the Mach number is controlled via the adaptable diffuser downstream the test section. In transonic tests, the perforated walls inhibit the application of optical flow visualisation techniques (e.q. schlieren).

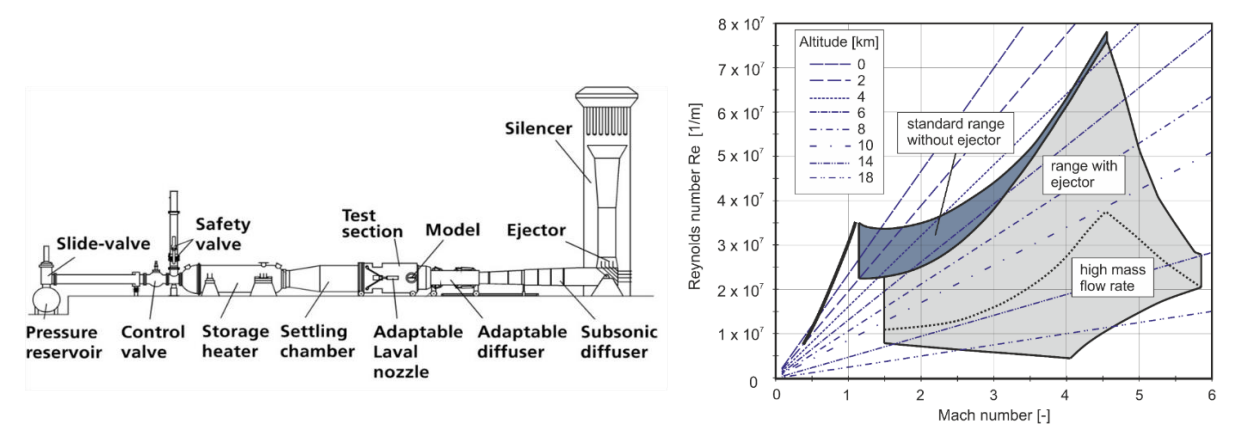


Fig. 4. Schematic (left) and performance map (right) of wind tunnel TMK

2.3. WIND TUNNEL MODELS

Fig. 5 shows the aeroshape of the GHGV-1 with its flaps and fins and the location of the Centre of Gravity (CoG). The length is L = 3.0 m and its weight m = 352.6 kg.

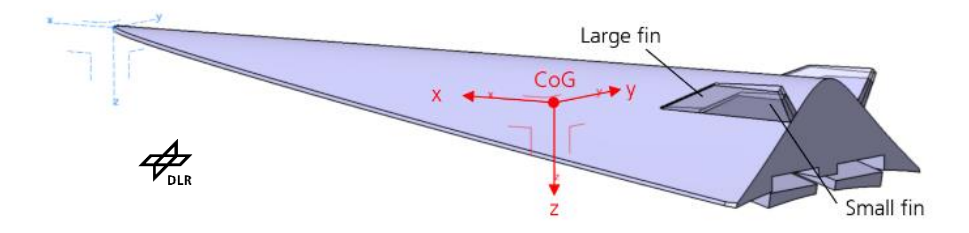


Fig. 5. Aeroshape of GHGV-1

For aerodynamic wind tunnel testing in the DLR facilities, the geometry is scaled down to 15%, i.e., the length of the wind tunnel model is $L_{model}=0.45~m$. Fig. 6 (left) shows the components of the static wind tunnel model for tests with an internal 6-component strain gauge balance. The balance adapter, model nose, fins and flaps are manufactured from steel whereby the model main body is manufactured from aluminium. Different sets of exchangeable fins $(0^{\circ}, \pm 10^{\circ}, \pm 20^{\circ})$ and flaps $(0^{\circ}, 5^{\circ}, 10^{\circ}, 20^{\circ})$ allow for aerodynamic testing of configurational aspects. One set of larger fins with a deflection of $+10^{\circ}$ (named 10a) was manufactured later to allow for a flap efficiency analysis.

The same scaling is used for the dynamic wind tunnel model shown in Fig. 6 (right). The model is equipped with just 2 sets of flaps $(0^\circ,1^\circ)$ and a system to adjust the fin deflection in the range -10° to $+10^\circ$ in steps of 2.5° . Two sets of fins (small and large) are manufactured. The image also shows the adapter for model alignment in the test section and the cross-spring used within the dynamic pitching motion tests. Design of the model ensures that the centre of gravity coincides with the CoG of the original GHGV-1 and doesn't change when exchanging flaps or fins.



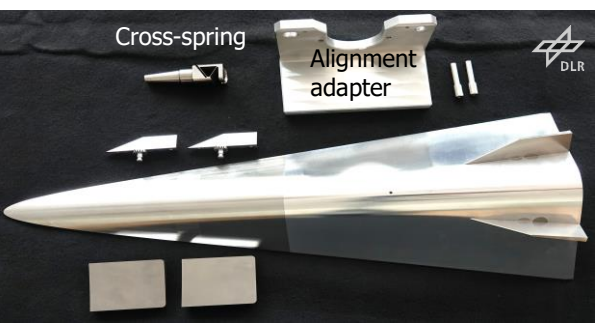


Fig. 6. Components of static (left) and dynamic wind tunnel model (right)

2.4. MEASUREMENT TECHNIQUE

Static aerodynamic measurements

Static aerodynamic forces and moments are measured in the wind tunnel to investigate the static stability of the aeroshape. A high-precision, six-component internal balance (either manufactured by DLR or a commercially available one) is used. The test model is mounted directly on the balance which is connected to a rigid sting support. Base pressure in the model's wake is measured with KULITE sensors. During testing, the incidence angle is altered to investigate complete polar curves. During post-processing, pressure sensor and balance calibration data are applied and aerodynamic coefficients according to Fig. 7 are calculated using the ratio of specific heats κ , Mach number Ma, stagnation pressure p_0 , model reference area ($S_{Ref} = 0.004924 \, m^2$) and characteristic length ($L_{Ref} = 0.07918 \, m$):

Force coefficients:
$$C_F = \frac{2 \cdot F}{\kappa \cdot M \alpha^2 \cdot p_0 \cdot S_{ref}} \left(1 + \frac{\kappa - 1}{2} \cdot M \alpha^2 \right)^{\frac{\kappa}{\kappa - 1}}$$
 (1)

Moment coefficients:
$$C_M = \frac{2 \cdot M}{\kappa \cdot M a^2 \cdot p_0 \cdot L_{ref} \cdot S_{ref}} \left(1 + \frac{\kappa - 1}{2} \cdot M a^2 \right)^{\frac{\kappa}{\kappa - 1}}$$
 (2)

Base pressure coefficient:
$$C_{pB} = \frac{p_B \cdot \left(1 + \frac{\kappa - 1}{2} M a^2\right)^{\frac{\kappa}{\kappa - 1}} - p_0}{\frac{\kappa}{2} M a^2 \cdot p_0}$$
 (3)

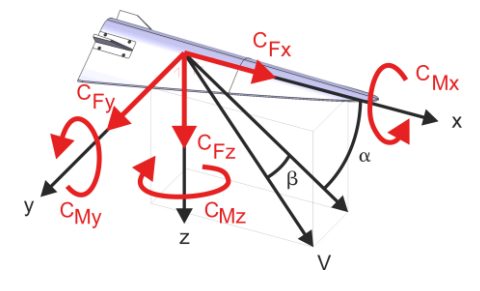


Fig. 7. Body fixed coordinate system and aerodynamic coefficients

Determination of derivatives

The applied method analyses free oscillations of the wind tunnel model with and without flow influence. Therefore, the model is fixed to a sting by means of a cross-spring and oscillates with one degree of freedom around its centre of gravity. As the pitch rate q is equal to the derivative $\dot{\alpha} = \dot{\theta}$, only the sum of damping coefficients $\mathcal{C}_{mq}+\mathcal{C}_{m\dot{\alpha}}$ and the aerodynamic stiffness $\mathcal{C}_{m\alpha}$ can be determined.

The motion of the model is considered as a small deflection relative to the trimmed position that is described by the following differential equation:

$$I_{\nu}\ddot{\theta} + (k_{\nu} - M_{\dot{\theta}})\dot{\theta} + (c_{\nu} - M_{\dot{\theta}})\theta = 0 \tag{4}$$

with I_y the moment of inertia, k_y the mechanical damping, c_y the mechanical stiffness, $M_{\dot{\theta}}$ the aerodynamic damping and M_{θ} the aerodynamic stiffness.

Using the common ansatz for a damped harmonic oscillation

$$\theta(t) = \theta_{defl} \, e^{-\delta t} e^{i\omega t} \tag{5}$$

with θ_{defl} the oscillation amplitude, δ the damping decrement and ω the angular frequency, the aerodynamic stiffness and damping coefficients can be calculated as:

$$M_{\theta} = -I_{y}(\omega^{2} + \delta^{2}) + c_{y} \rightarrow C_{m\alpha} = \frac{M_{\theta}}{\frac{\rho_{\infty}}{2} u_{\infty}^{2} S_{Ref} L_{Ref}},$$
(6)

$$M_{\dot{\theta}} = -2I_{y}\delta + k_{y} \rightarrow \left(C_{mq} + C_{m\dot{\alpha}}\right) = \frac{M_{\dot{\theta}} \cdot u_{\infty}}{\frac{2}{2}u_{\infty}^{2} S_{Ref}L_{Ref}^{2}},\tag{7}$$

with ρ_{∞} and u_{∞} representing the density and velocity of the free stream, and S_{ref} and L_{ref} the model reference parameters.

Further information about the free oscillation technique, calibration procedure of the cross-spring and data analysis process can be found in [6, 7]

2.5. FLOW VISUALISATION TECHNIQUE

Visualizing flow structures is important for understanding flow phenomena and for validating numerical simulations, not just through calculated force and moment coefficients but also through the comparison of the flow topology. In supersonic flows, shock waves and expansion fans can be made visible using the <u>Schlieren technique</u>. This involves passing parallel light through the test section, refocusing it before it reaches the camera, and using a knife edge to block light deflected by density gradients (caused by refractive index changes). Areas where light is blocked appear dark in the image. In the Schlieren images shown in this report, these dark regions correspond to shock waves or weaker disturbances known as Mach lines. The Schlieren technique is a standard measurement method used in aerodynamic tests at both the H2K and TMK facilities. Depending on the camera system, up to 5 high-resolution images per second are captured, and the correlation with the angle of attack is performed via software-based edge detection.

The <u>oil-film technique</u> is applied to reveal surface streamlines at selected test conditions. For these tests, the model's balance is replaced with a rigid adapter, and the model is aligned in the wind tunnel at the desired angle of attack (and sideslip, if needed), accounting for possible elastic deflection under aerodynamic loads. A mixture of oil and pigment—its viscosity adjusted to test conditions—is applied over the entire model surface. The test is then immediately started and conditions are held steady until the oil film dries. Afterwards, the model is removed and photographed from all sides. As the film is redistributed by shear forces during the test, vortex structures or separated flow regions can be identified from these patterns, though interpretation is not always unambiguous.

3. STATIC EXPERIMENTAL TEST CAMPAIGN

Aerodynamic testing is performed in both DLR facilities H2K and TMK to cover a wide Mach range from Ma=8.8 down to Ma=2. Fig. 8 shows the GHGV-1 model in the open test section of H2K (left) and the closed test section of TMK (right). At wind tunnel start-up and shut-down, the balance is aligned horizontally, i.e. the GHGV-1 model has an angle of attack of $\alpha=-3^\circ$. After flow has established, the model is first driven to an angle of attack of $\alpha\approx-5^\circ$ and then to $\alpha\approx+13^\circ$ (H2K) or $\alpha\approx+10^\circ$ (TMK) and back to $\alpha\approx-3^\circ$. Finally, the flow is switched off. From the recorded balance signals, the aerodynamic coefficients are calculated according to section 2.4

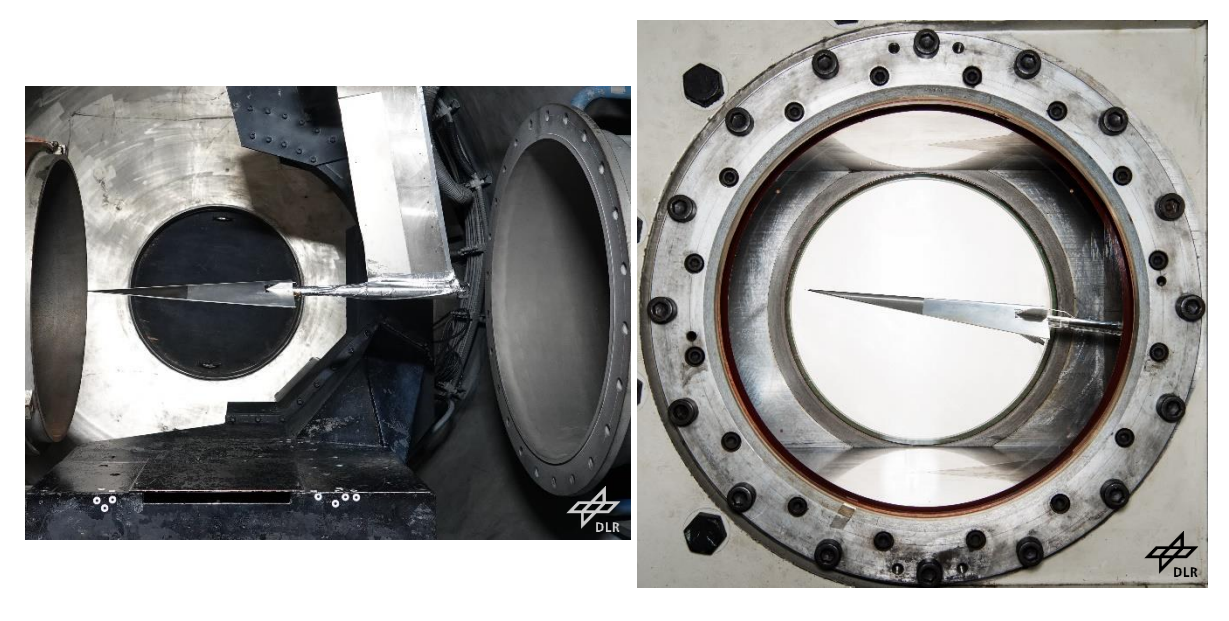


Fig. 8. GHGV-1 model in test section of H2K (left) and TMK (right)

3.1. TEST MATRIX

Fehler! Verweisquelle konnte nicht gefunden werden. gives an overview on the tests performed in H2K ($Ma \ge 5.3$) and TMK. In total, 76 aerodynamic tests in H2K and 73 tests in TMK are conducted to address trim ability of the vehicle, efficiency of control surfaces and the effect of sideslip and bank angle. Additionally, 6 tests in TMK are dedicated to a visualisation of surface stream lines applying the oil film technique. Simulation results are available for the configurations marked accordingly.

Tahla 1	Test matrix	of static	aerodyna	mic tosts
i abie 1.	rest matrix	UI SLALIC	aerouviia	IIIIC LESIS

UL[°]	UR [°]	LL [°]	LR [°]	Ma = 8.8	Ma=7.1	Ma=5.3	Ma=4.0 Ma=3.0		Ma=2.0
0	0	0	0	ReH,M,L	ReLβ0,-3	ReH,ReLβ0,-3	φ0,-5,-90	φ0,-5,-90	φ0,-5,-90
0	0	5	5		ReL	ReL	φ0,-5,-90	φ0,-5,-90	φ0,-5,-90
0	0	10	10	ReH	ReLβ0,-3	ReH,ReLβ0,-3	Х	Х	Х
0	0	20	20	ReH,M,L	ReL	ReH,L	х	х	х
10	10	0	0	ReH	ReL	ReH,L	х	Х	Х
20	20	0	0	ReH	ReL	ReL	х	Х	х
-10	-10	0	0	ReH	ReL	ReL	х	х	х
-20	-20	0	0		ReL	ReL	х	х	х
10a	10a	0	0	ReH	ReL	ReL			
0	0	0	5		ReL	ReL	х	х	х
0	0	0	10	ReH	ReL	ReL	х	Х	Х
0	0	0	20	ReH	ReL	ReL	х	х	х
10	0	0	0	ReH	ReL	ReL	х	х	х
20	0	0	0	ReH	ReL	ReL	х	х	х
0	-10	0	0	ReH	ReL	ReL	х	х	Х
0	-20	0	0		ReL	ReL	х	х	х
10a	0	0	0	ReH	ReL	ReL			
10	0	0	5				х	х	х
10	0	0	10			ReL	х	х	х
10a	0	0	10			ReL			
10	-10	0	5				х	х	х
10	-10	0	10			ReH,L	х	х	х
-10	10	0	0		ReLβ-3	ReLβ-3			
10	-10	0	0		ReLβ-3	ReLβ-3			
10	-10	10	0			ReLβ-3			
10	-10	20	0			ReLβ-3			

Nomenclature:

deflection left fin UI deflection right fin UR LL deflection left flap deflection right flap LR ReH high Reynolds number ReM medium Reynolds number low Reynolds number ReL sideslip angle of β =0 β0 β-3 sideslip angle of $\beta\text{=-}3^{\circ}$ roll angle of ϕ =0° φ0 φ-5 roll angle of ϕ =-5° φ-90 roll angle of ϕ =-90° unmarked $\beta=0^{\circ}$, $\phi=0^{\circ}$ Num. simulation data

HiSST-2025-0013 Aerodynamic wind tunnel testing of a generic Hypersonic Glide Vehicle

3.2. IMPACT OF MACH NUMBER

One important outcome of the investigation is the Mach number dependency of the aerodynamic coefficients which justifies extension of the investigation to a relatively broad Mach range. Exemplarily, the experimentally determined aerodynamic coefficients for the configuration UL00UR00_LL10LR10, i.e. for 0° fin and 10° flap deflection are shown in Fig. 9. The coefficients relevant for analysis of the longitudinal movement and the lift-to-drag ratio are plotted against the angle of attack α .

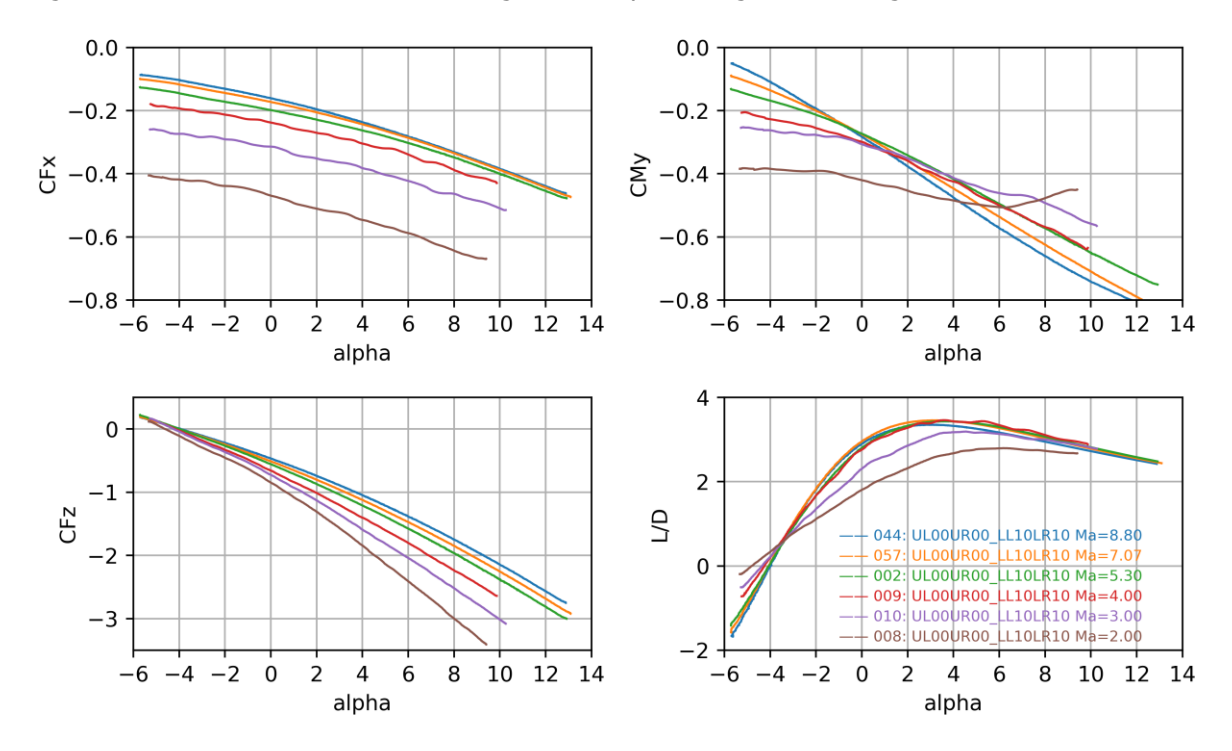


Fig. 9. Impact of Mach number on aerodynamic coefficients

The diagrams show that increasing the angle of attack α increases the absolute values of the force coefficients C_{Fx} and C_{Fz} for all Mach numbers. At a constant α , lower Mach numbers lead to higher absolute C_{Fx} and C_{Fz} values. The curves of the normal force coefficient C_{Fz} intersect around $\alpha \approx -4^{\circ}$, except for Ma=2, and diverge with increasing α . The pitching moment coefficient C_{My} decreases monotonically with α for $Ma \geq 5.3$. As trim points are reached with almost no flap deflection, none of the curves shown here achieves positive values of C_{My} . Obviously, the transit from hypersonic to supersonic noticeably changes the pitch behaviour of the vehicle as shown by the change in curve characteristic when decreasing the Mach number.

Lift-to-drag ratio L/D indicates the gliding performance of the vehicle, peaking with L/D>3 for Mach numbers $Ma\geq 4$ at $\alpha\approx +3^\circ$. Higher values above 4 are achieved without control surface deflection (not shown). At lower Mach numbers, the L/D ratio decreases and the maximum is shifted to $\alpha\approx 6^\circ$ at Ma=2.

3.3. CONTROL SURFACE EFFICIENCY

Control of the vehicles flight path in the atmosphere is performed by using the upper fins and lower flaps. Therefore, the efficiency of the control surfaces is of high interest with respect to the mission scenario and the Guidance, Navigation and Control (GNC). The results presented in this section are obtained from experiments with the small set of fins at a test Mach number of Ma = 7.1. The results are presented in comparison to numerical data of a 3D Euler simulation with the DLR flow solver TAU, performed during the *Design Phase* of the vehicle. Selected tests are performed with the set of large fins to also allow for a validation of the numerical simulations for large fins (not shown here).

Fig. 10 shows the complete set of aerodynamic coefficients for selected configurations that focus on the deflection of one single control surface only. The solid lines represent the experimental data and

the dashed lines the results from numerical simulation. During the campaign it has been found that the combination of different deflected control surfaces can be fairly good estimated by application of the superposition principle.

The black curves in the viewgraphs represent the baseline configuration without fin or flap deflection UL00UR00_LL00_LR00 as reference to judge the coefficient change due to the deflected control surface. Except for the axial force coefficient $C_{\rm Fx}$, a fairly good coincidence is observed between experiment and numerical simulation. The experimentally determined $C_{\rm Fx}$ shows slightly higher absolute values than the numerically calculated. This seems to be a general trend that applies to the other test cases shown here as well.

The right flap deflected to 20° gives the aerodynamic behaviour shown in blue. It is obvious that deflection of this control surface has a significant impact on all coefficients and that this impact increases with angle of attack. In contrast, deflection of the left fin to $+20^\circ$ (red curves) or the right fin to -20° (green curves), to achieve an effect in the same direction, shows an impact on all coefficients, too, but, expectedly, that decreases with increasing angle of attack, due to the "shadowing" effect of the vehicle's fuselage.

The general trends are reproduced by the numerical simulation for all four configurations, but deviations can be found in the details. One reason might be that friction is not accounted for by Euler calculations, although a viscous correction has been applied. Another reason might be an uncorrected impact of the model support on the experimental results. On the whole, the outcome of the comparison supports the chosen approach to first evaluate the vehicle's design with relatively simple und computationally inexpensive numerical simulations, then build up an experimental database and finally perform more sophisticated simulations for selected test cases.

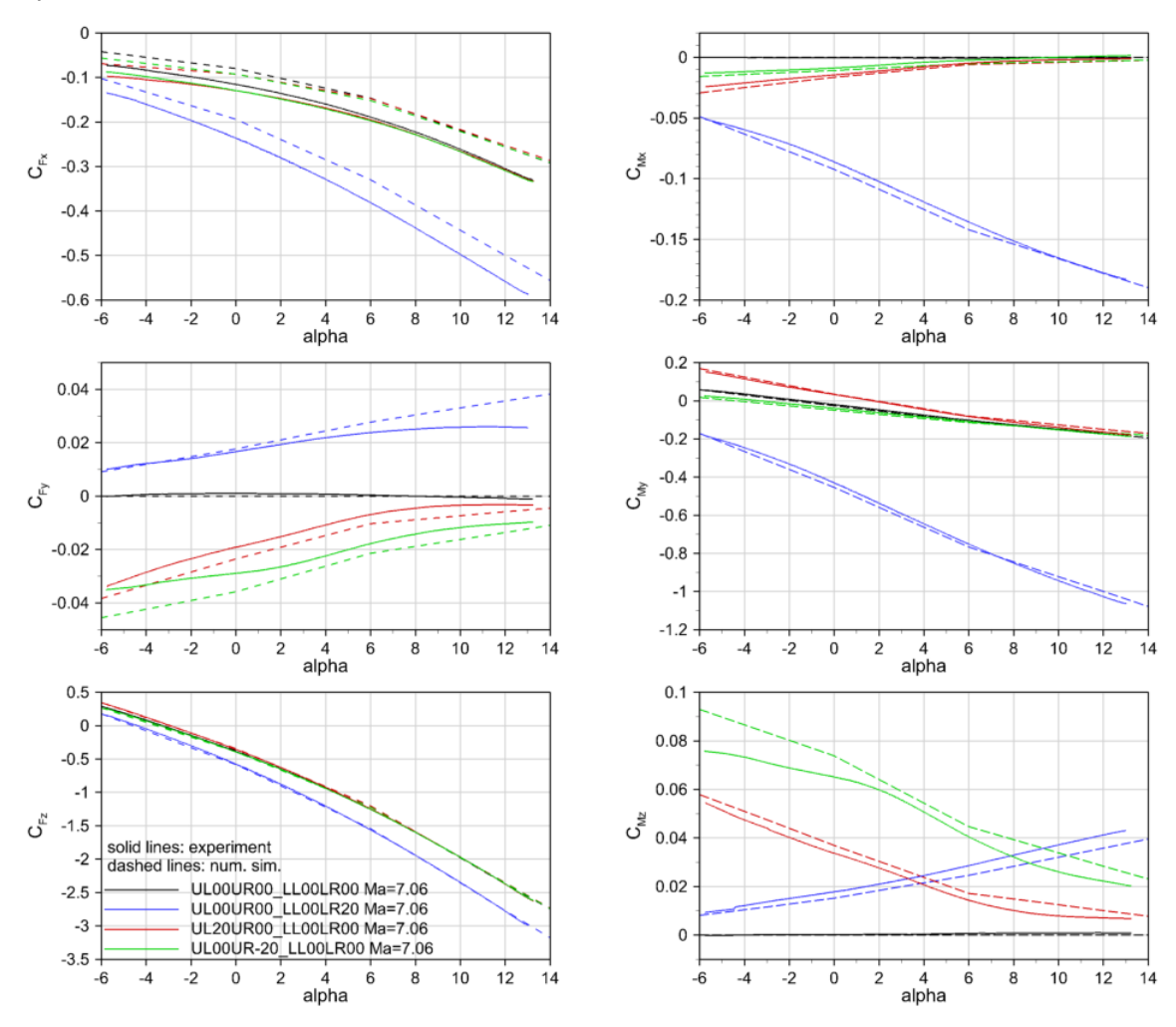


Fig. 10. Control surface efficiency in experiment and numerical simulation

4. DYNAMIC EXPERIMENTAL TEST CAMPAIGN

A special mechanism has been developed to perform dynamic free oscillation tests with different wind tunnel models [8-10]. As in the current case the pitch rotation axis is very close to the model outer contour, a special cross-spring with off-centre rotation axis has been developed [11, 12]. The spring is equipped with strain-gauges to measure the deflection. The mechanism with cross-spring in its different test states is shown in Fig. 11, as CAD-sketch on top and photographs without wind tunnel model below.

Within a dynamic wind tunnel test, the sting angle, considering the pretended sting bending due to aerodynamic forces and moments, is set prior to wind tunnel start-up. The mechanism is set to status a), fixing the model on the sting with the pins on top and bottom side of the model. The mechanism is in its rightmost position. Moving the mechanism to the left, the model is first deflected (status b) and released suddenly when the mechanism reaches status c). The model oscillates freely for a defined time span. Then, the mechanism is moved rightwards and the model is captured at status d) and deflected again. A sliding mechanism thereby provides the sudden release in one direction and a smooth capture in the other direction. The release can be repeated (status c) or the model fixed to the sting (status a).

The test procedure is performed first without wind tunnel flow (Dry run) to determine the reference parameter. Then, the real test is performed (Run) usually deflecting and releasing the model several times during one run. Applying the coefficients of the prior performed static and dynamic calibration of the cross-spring, the dynamic derivates can be calculated as described in section 2.4.

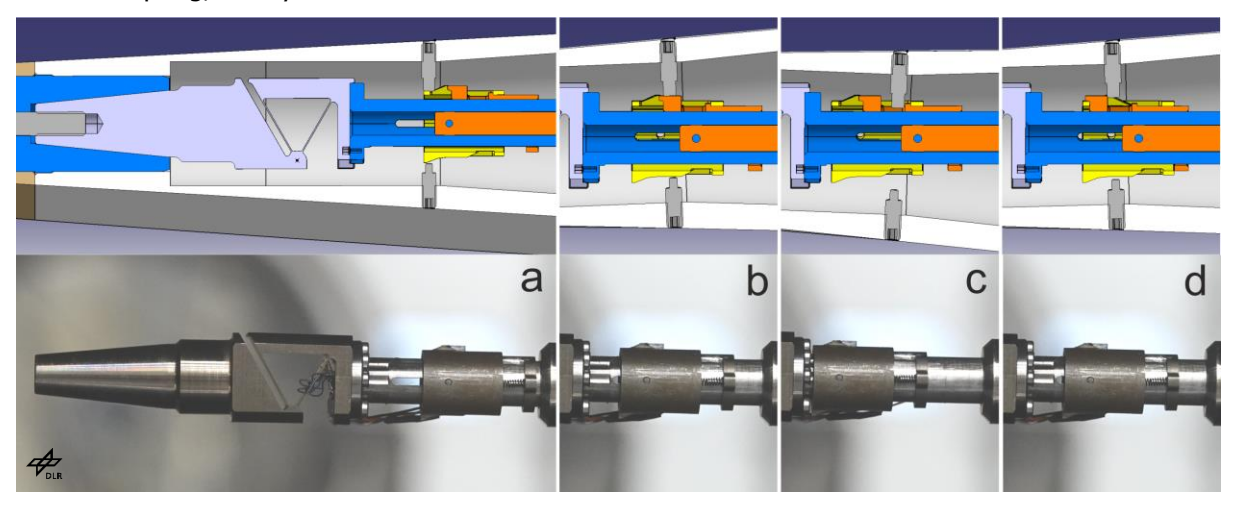


Fig. 11. Mechanism for dynamic testing, a) model fixed, b) deflected, c) released, d) captured

4.1. TEST MATRIX

Dynamic testing was performed with both sets of fins, small and large. The configurations, Mach number Ma, the aligned angle of attack α_0 and the determined trim angle α_{trim} are given in Table 2. One test at Ma=5.3 with small fins and without deflected control surfaces was repeated to prove reproducibility. Deviation in the trim angle in these two tests is very small with $\alpha \leq 0.1^{\circ}$.

It was decided to concentrate on the large fins for the future. Therefore, a reduced program was performed with the small fins and the fin deflection of $\pm 5^{\circ}$ was investigated with large fins only. The table clearly shows, that changing to the set of large fins has a significant impact on the trim angle, even for non-deflected fins. The higher fin efficiency of the larger fins allows for a flight path control that requires smaller fin deflection angles.

The configuration with small fins and non-deflected control surfaces yields a trim angle of $\alpha_{trim} \approx -1.52^{\circ}$ at Ma = 5.3, but of $\alpha_{trim} = -0.86^{\circ}$ at Ma = 7.1. In contrast, large fins with non-deflected control surfaces yield a trim angle of $\alpha_{trim} \approx -1.02^{\circ}$ at both, Ma = 5.3 and 7.1. Within dynamic testing, only small flap deflections of 1° were combined with fin deflections in the range $\pm 10^{\circ}$. For the small fins this yields a trim angle of $-5.69^{\circ} \leq \alpha_{trim} \leq 1.54^{\circ}$ and for the large fins in the range $-7.3^{\circ} \leq \alpha_{trim} \leq 3.15^{\circ}$.

	Small fins					Large fins							
UL[°]	UR [°]	LL [°]	LR [°]	Ma	α ₀ [°]	α_{trim} [°]	UL[°]	UR [°]	LL [°]	LR [°]	Ma	α ₀ [°]	α_{trim} [°]
-10	-10	0	0	5.3	-4.52	-4.45	-10	-10	0	0	5.3	-6.44	-6.51
							-5	-5	0	0	5.3	-3.54	-3.51
0	0	0	0	5.3	-1.58	-1.52 -1.53	0	0	0	0	5.3	-1.05	-1.02
							5	5	0	0	5.3	1.03	1.11
10	10	0	0	5.3	1.55	1.54	10	10	0	0	5.3	3.19	3.15
-10	-10	1	1	5.3	-5.80	-5.69	-10	-10	1	1	5.3	-7.31	-7.30
							-5	-5	1	1	5.3	-4.63	-4.53
0	0	1	1	5.3	-2.96	-2.79	0	0	1	1	5.3	-2.06	-2.00
							5	5	1	1	5.3	0.20	0.24
10	10	1	1	5.3	0.24	0.33	10	10	1	1	5.3	2.26	2.30
-10	-10	0	0	7.1	-3.50	-3.41	-10	-10	0	0	7.1	-5.07	-4.98
							-5	-5	0	0	7.1	-2.03	-2.11
0	0	0	0	7.1	-0.80	-0.86	0	0	0	0	7.1	-1.04	-1.01
							5	5	0	0	7.1	1.69	1.61
10	10	0	0	7.1	1.08	1.14	10	10	0	0	7.1	2.26	2.33
-10	-10	1	1	7.1	-4.47	-4.30	-10	-10	1	1	7.1	-6.05	-5.92
							-5	-5	1	1	7.1	-3.02	-2.93
0	0	1	1	7.1	-1.47	-1.54	0	0	1	1	7.1	-1.52	-1.55
							5	5	1	1	7.1	0.28	0.29
10	10	1	1	7.1	0.14	0.29	10	10	1	1	7.1	1.39	1.52

Table 2 Test matrix of dynamic free oscillation tests

4.2. DATA ANALYSIS

As described above, the model oscillation is recorded with and without flow influence. Exemplarily, Fig. 12 shows recorded oscillations of two different tests. The model is first deflected to about 2° and then released. As the model oscillates freely, the motion is very near to a harmonic oscillation and can be rebuilt accordingly to determine the oscillation frequency and the damping.

As the viewgraphs show, the oscillation frequency in the Dry run (grey curves) is both times lower than during the Run with wind on (black curves), i.e. the model's aerodynamic increases the stiffness of the system. The same accounts for the damping which is also increased through aerodynamic effects. Analysis of the oscillation change gives as results the desired dynamic derivatives.

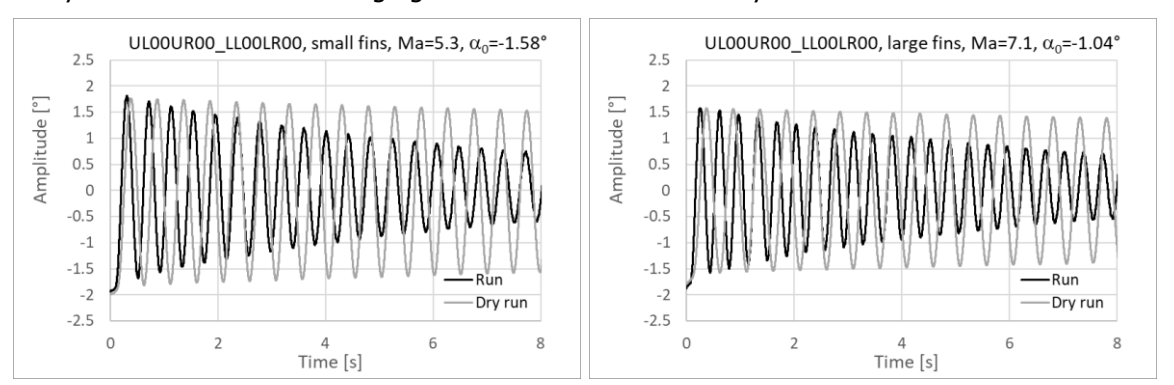


Fig. 12. Model oscillation in Run and Dry run, UL00UR00_LL00LR00, Ma=5.3, small fins (left) and Ma=7.1, large fins (right)

4.3. DYNAMIC DERIVATES AT HYPERSONIC CONDITIONS

Fig. 13 presents the results from the dynamic stability investigations carried out in the H2K wind tunnel for test Mach numbers Ma=5.3 and 7.1. The top row shows the derivatives for configurations with small fins and the bottom row for configurations with large fins. By rebuilding the model motion as a damped harmonic oscillation, the analysis provides not only the dynamic derivatives shown, but also an offset from the actual trim angle. This offset allows the true trim angle to be determined with an accuracy of approximately $\pm 0.2^{\circ}$. In the diagram, the results are plotted against the calculated actual trim angle α_{trim} .

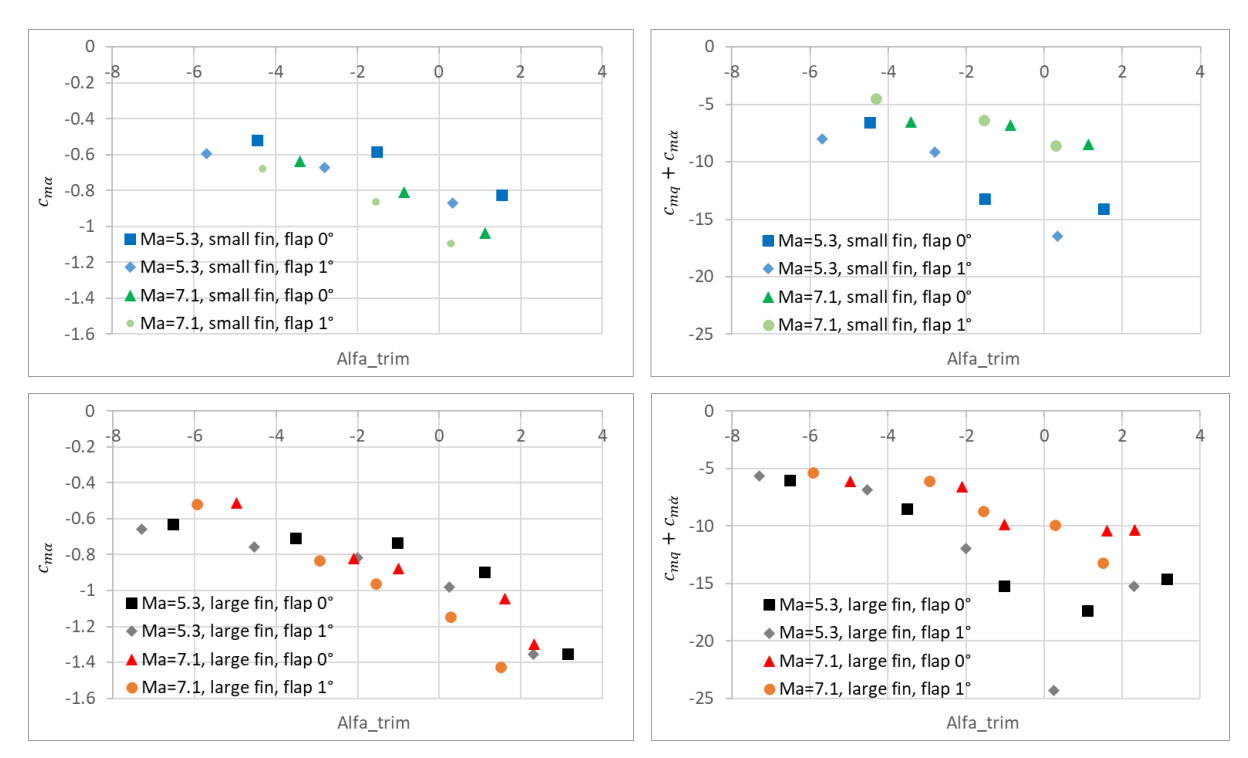


Fig. 13. Dynamic derivatives at Ma = 5.3 and 7.1

As primary observation both dynamic derivatives, aerodynamic stiffness $C_{m\alpha}$ and damping $C_{mq} + C_{m\dot{\alpha}}$, are negative for all investigated test conditions/configurations. This means that the GHGV-1 vehicle is not only statically stable in the investigated Mach range, but also dynamically stable. This means that any small perturbation from a trimmed condition causes a damped oscillation with the model returning to the trimmed condition. Second observation gives a slightly higher aerodynamic stiffness for the large fins whereby damping is not significantly changed. This shows, that the impact of the control surfaces on the dynamic derivatives is primarily related to the change in angle of incidence and not to the stiffness/damping impact of the surface itself.

5. FLOW VISUALISATION

5.1. SCHLIEREN IMAGES

This visualisation technique gives valuable information about flow structures and is usually applied in static and dynamic wind tunnel tests. In Fig. 14, Schlieren images for different configurations are shown at an inflow Mach number of Ma=4 and an angle of attack of $\alpha\approx +3.5^{\circ}$. The left image shows the impact of a $+10^{\circ}$ fin deflection (UL10UR10_LL00LR00), the centre image of a 5° flap deflection (UL00UR00_LL05LR05) and on the right, the flow structure of a combined deflection (UL10UR10_LL05LR05) is visible that pretty much resembles a superposition of the two other images.

The details in the lower row of the image clearly show the shock waves in compression regions and as well minor gradients (Mach lines) that are caused at surface discontinuities like the junction between model nose and main body or the upstream edge of the flap inserts. Although visible, their effect on aerodynamics is negligible.

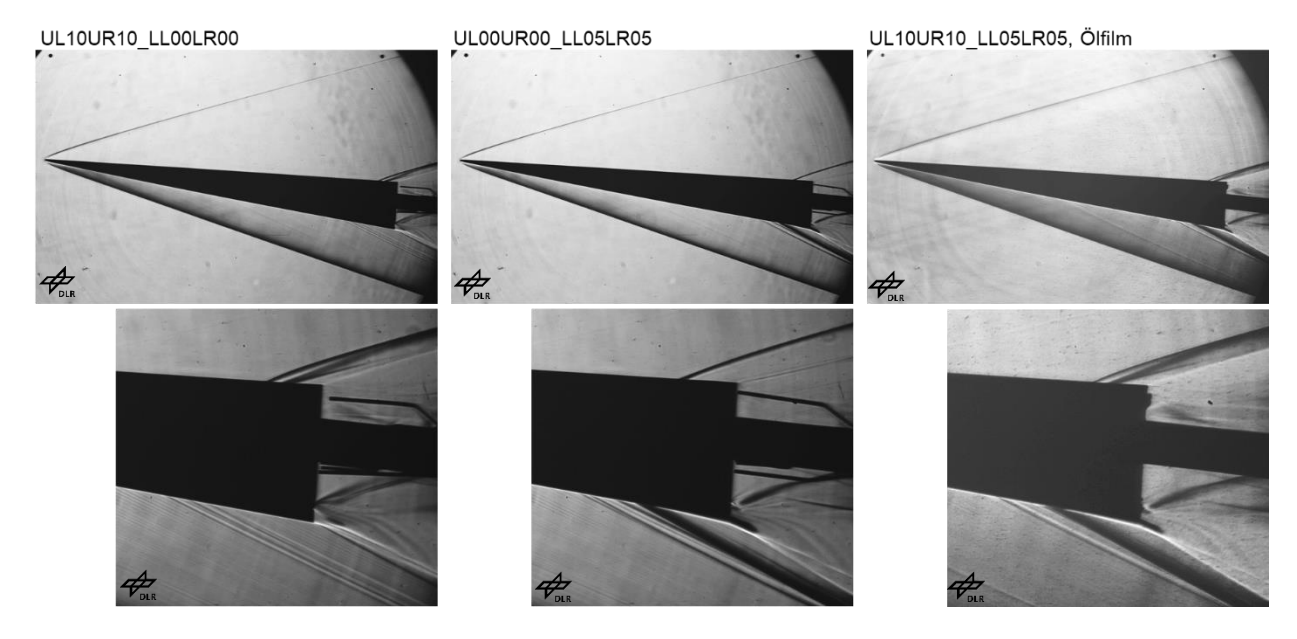


Fig. 14. Schlieren images at Ma = 4, $\alpha \approx +3.5^{\circ}$

5.2. OIL FLOW IMAGES

Fig. 15 shows the oil flow images recorded after tests at Ma=4. On the left, configuration UL10UR10_LL05LR05, tested at an angle of attack of $\alpha\!pprox\!+3.5^\circ$ is shown (see corresponding Schlieren images in Fig. 14, right). From the streamlines, the flow deflection between the fins is visible. On the leeward side of the fins, the structure is difficult to interpret. It could be a flow separation maybe in combination with a vortex. Additionally, on the upper side, a redirection of the streamlines in outward direction can be observed.

On the right, configuration UL00UR00_LL05LR05 after a test at $\alpha \approx -3^{\circ}$, $\beta \approx -2^{\circ}$ is shown. In this case, the streamlines clearly indicate the impact of sideslip during the test which counteracts the outward flow direction on the left model surface near the base: streamlines are now oriented along the vehicle. Concerning the fins, the no-deflection in combination with a sideslip angle leads to the visible impact on the direction of the streamlines in the vicinity of the fins.

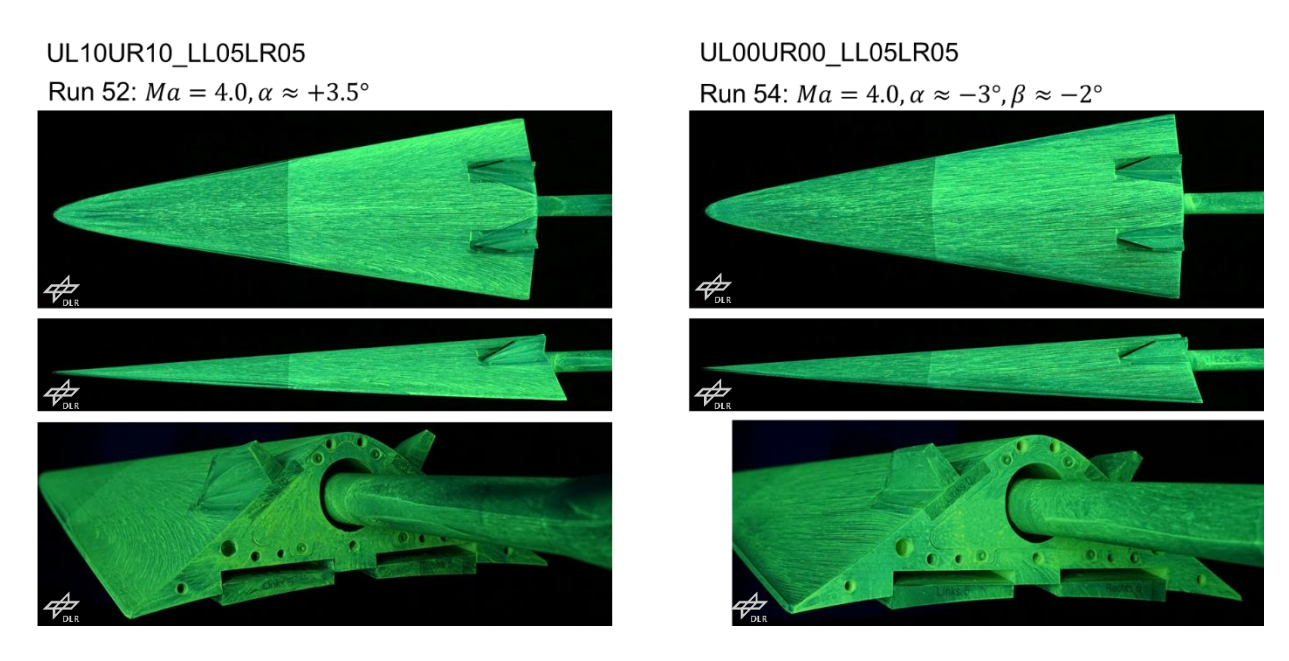


Fig. 15. Oil flow images at Ma = 4

6. CONCLUSION

The aerodynamic performance of the GHGV-1 vehicle is topic of an ongoing research at DLR. Design was made in house and evaluated first with Euler simulations using the DLR TAU code. Then, a wind tunnel model was built and static aerodynamic tests were performed in a wide Mach number range (Ma = 8.8 to Ma = 2.0). Experimental results were compared with the simulation data. The model proved static stability in the studied range and aerodynamic coefficients of simulation and experiment were determined in acceptable accordance. Only selected results of this study could be presented within this publication like the Mach number dependency of the aerodynamic coefficients or the efficiency of single deflected control surfaces in comparison to the numerical prediction.

A second wind tunnel model was built to perform dynamic stability tests with the free oscillation technique. First tests were performed successfully in the Hypersonic wind tunnel Cologne using an existing dynamic test mechanism together with a specially designed cross-spring with an off-centre rotation axis. At Ma = 5.3 and Ma = 7.1, the aerodynamic stiffness and damping were both found to be negative for several investigated trim conditions around the trim point of the baseline configuration (no deflected control surfaces). This proves the GHGV-1 vehicle's aerodynamic behaviour to be statically and dynamically stable within the design flight envelope.

A brief flow structure analysis based on Schlieren images and oil flow visualisations was presented as well. Both techniques proved valuable to provide additional data for a validation of CFD simulations, especially in cases where differences between the experiment and numerical simulations occur.

Extension of the dynamic experimental data base to lower Mach numbers is already under preparation, but expected loads are far too high for performing them with the existing apparatus. Therefore, a stronger apparatus is designed and built to be used with the existing wind tunnel model. Further on, investigation of the dynamic roll behaviour of the vehicle is planned. A test apparatus for application in H2K conditions ($Ma \ge 5.3$) is already existing.

The study of the GHGV-1 aeroshape is very comprehensive and includes multiple disciplines from design to simulation and experiment to analysis. This systematic investigation of the GHGV-1 vehicle does not only provide information about these types of potential threats but also improves application of the different techniques in such a combined study.

7. REFERENCES

- [1] Patrick Gruhn *et al.*, "Design and analysis of generic hypersonic glide vehicles," presented at the NATO STO AVT-SET-396 Research Symposium on "Technological Challenges due to Hypersonic Flight and the related Weapons Threat", Koblenz, Germany, October 14-17, 2024.
- [2] Thomas Gawehn, Junnai Zhai, Patrick Gruhn, and Ali Gülhan, "Aerodynamic wind tunnel testing on the Generic Hypersonic Glide Vehicle 1 (GHGV-1)," presented at the NATO STO AVT-SET-396 Research Symposium on "Technological Challenges due to Hypersonic Flight and the related Weapons Threat", Koblenz, Germany, October 14-17, 2024.
- [3] Thomas Gawehn and Junnai Zhai, "Untersuchungen zur statischen Stabilität des GHGV-1," Institut for Aerodynamics and Flow Technology, Cologne, Internal Report DLR-IB-AS-KP-2024-132, 27. August, 2024.
- [4] F.-J. Niezgodka, "Der Hyperschallwindkanal H2K des DLR in Köln-Porz (Stand 2000)," Institut für Aerodynamik und Strömungstechnik, Abteilung Windkanäle, Köln-Porz, 2002.
- [5] Helmut Esch, "Die 0.6-m x 0.6-m-Trisonische Meßstrecke (TMK) der DFVLR in Köln-Porz (Stand 1986)," DFVLR, Hauptabteilung Windkanäle, Köln, Mitteilung DRVLR-Mitt. 86-21, 1986.
- [6] Thomas Gawehn and Ali Gülhan, "Experimental Study on Static and Dynamic Stability of a Blunt Body Configuration," presented at the International Conference on Flight Vehicles, Aerothermodynamics and Re-entry Missions & Engineering (FAR 2019), Monopoli, Italy, 2019. [Online]. Available: https://elib.dlr.de/129437/.
- [7] Ali Gülhan, Josef Klevanski, and Thomas Gawehn, "Experimental Study on the Dynamic Stability of the IXV Configuration," presented at the 8th European Symposium on Aerothermodynamics for Space Vehicles, Lissabon, Portugal, March 2-6, 2015. [Online]. Available: https://elib.dlr.de/98422/.

- [8] Thomas Gawehn, Junnai Zhai, and Markus Miketta, "Wind tunnel test device for determining dynamic invalties at a wind tunnel model", European Patent, Patent Number: 25 154 661.0, Europe, 2025.
- [9] Thomas Gawehn, Junnai Zhai, and Markus Miketta, "Windkanaltestvorrichtung zur Ermittlung von Dynamischen Beiwerten an einem Windkanalmodell", Deutsches Patent, Patent Number: 10 2024 102 388.0, Germany 2024.
- [10] Junnai Zhai, Thomas Gawehn, and Ali Gülhan, "Dynamic stability testing in DLR Wind Tunnels using a new free oscillation device" presented at the 4th International Conference on High-Speed Vehicle Science Technology, Tours, September 22-26, 2025.
- [11] Thomas Gawehn, Junnai Zhai, and Markus Miketta, "Federvorrichtung für Schwingbewegungen von Modellen sowie Windkanaltestvorrichtung mit Federvorrichtung", European Patent, Patent Number: 25192073.2, Europe, 2025.
- [12] Thomas Gawehn, Junnai Zhai, and Markus Miketta, "Federvorrichtung für Schwingbewegungen von Modellen sowie Windkanaltestvorrichtung mit Federvorrichtung", Deutsches Patent, Patent Number: 10 2024 121 618.2, Germany 2024.